Dynamics of Haines Jumps for Compressible Bubbles in Constricted Capillaries

The unsteady, impulsive motion of a compressible bubble expanding out of a constricted capillary is quantified with a macroscopic momentum balance. Numerical solution demonstrates the importance of the Ohnesorge number, the geometry of the constriction, the length of the initial gas bubble, and the surface tension, density, and unconstricted capillary radius, which combine to form a characteristic scaling time. Experimental data for the position of the bubble front as a function of time confirm the theoretical result when the time scale for the bubble jump is longer than that required to achieve fully developed parabolic flow. Theory also predicts the capillary number of the bubble jump which, in conjunction with previous theoretical results, determines the time to snap-off of gas bubbles moving through constricted capillaries. Excellent agreement is found with existing experimental data for Ohnesorge numbers ranging from 5×10^{-3} to 0.3.

P. A. Gauglitz, C. J. Radke
Chemical Engineering Department
University of California
Berkeley, CA 94720

Introduction

The unsteady, impulsive advance of the front of nonwetting drops in porous media is well known and commonly called a Haines jump (Morrow, 1970). Haines jumps are also important when a nonwetting phase invades a water-wet porous medium along the drainage curve relating the capillary pressure (Adamson, 1976) to the liquid saturation (Craig, 1971). In this work, we study the impulsive motion of a compressible gas bubble moving through a smoothly constricted capillary. Since bubbles can change their length by compressing or expanding, their motion is affected by the gas compressibility.

In a recent experimental study, Gauglitz et al. (1988) determined that gas compressibility is important in quantifying gas-bubble snap-off in constricted cylindrical capillaries. Snap-off refers to breakup of the nonwetting phase at the neck of a constriction due to the wetting phase collecting there and blocking the pore. Snap-off of small bubbles or drops has important application in enhancing oil recovery with foams where the movement of discrete bubbles and drops is encountered (Falls et al., 1988; Hirasaki and Lawson, 1985).

The important steps in bubble snap-off are depicted in Figure 1. In the first two steps, the nonwetting bubble deposits a film of liquid which wets the walls of the capillary. The bubble continues to move forward, often via a rapid Haines jump downstream of the constriction, as indicated in step 3 of the figure. Liquid flows along the wetting films into a collar that gathers liquid at the neck of the constriction. Eventually, the collar collects enough liquid and rearranges into a liquid lens that blocks the pore. This is bubble snap-off, and is shown in step 4.

The movement of compressible bubbles through constricted cylindrical capillaries is reported by Gauglitz (1986) and Gauglitz et al. (1988) where 16 mm motion pictures record the bubble motion. The characteristics of many observations are depicted in Figure 2. The bubble is driven through the capillary by the wetting fluid, which is injected at a constant volumetric rate, as indicated by the parabolic velocity profile at the tube inlet for each capillary in Figure 2. As the bubble moves through the straight section of the capillary, upstream from the constriction, its velocity is constant. The pressure in the bubble increases when the front moves into the constriction due to surface tension forces and the curvature of the bubble front. Hence, the bubble volume must decrease in accordance with its increase in pressure. This occurs by the velocity of the bubble front slowing down while the rear of the bubble continues to move at a constant velocity. The decrease in bubble-front velocity is indicated in Figure 2 by the velocity profile at the tube exit. For the bubble to move past the neck of the constriction, it must achieve a pressure in excess of the capillary entry pressure (Craig, 1971). The bubble volume is smallest at the capillary entry pressure where the bubble front is at the neck of the constriction. Once the bubble front moves past the neck of the constriction, the expanding

Correspondence concerning this paper should be addressed to C.J. Radke.
P.A. Gauglitz is currently with Chevron Oil Field Research Company.

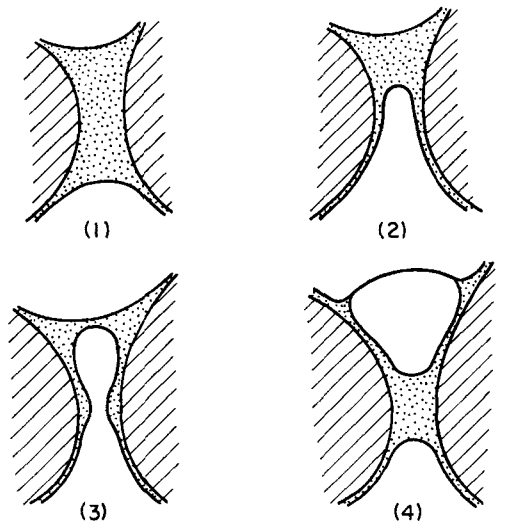

Figure 1. Pore level view of bubble generation by snap off.

gas pushes the bubble into the downstream section of the capillary. This motion is a rapid Haines jump (Morrow, 1970), labeled *Bubble Jump* in Figure 2.

Figure 3 plots an experimental example of an air bubble jump. The position of a bubble front from the neck of a constriction is shown as a function of time. The bubble front was essentially at rest in the neck of the constriction prior to the rapid movement shown in Figure 3. The bubble moves quickly out of the constriction, overshoots its final position, and then oscillates backward and forward. The volumetric flow of the injected fluid was very small in this experiment.

In a series of other investigations (Gauglitz, 1986; Gauglitz et al., 1988; Gauglitz and Radke, 1987), it is shown that the bubble velocity is crucial in determining the time required for the collar to snap off and the size of the generated bubble. These are important parameters for determining foam texture (bubble size and number density of bubbles) and for eventually understanding foam flow through porous media, which has important applications in enhancing oil recovery (Falls et al., 1988; Ransohoff, 1986; Friedmann and Jensen, 1986; Hirasaki and Lawson, 1985).

The bubble velocity is important because the capillary number, $Ca = \mu U/\sigma$, where U is the bubble velocity, determines the

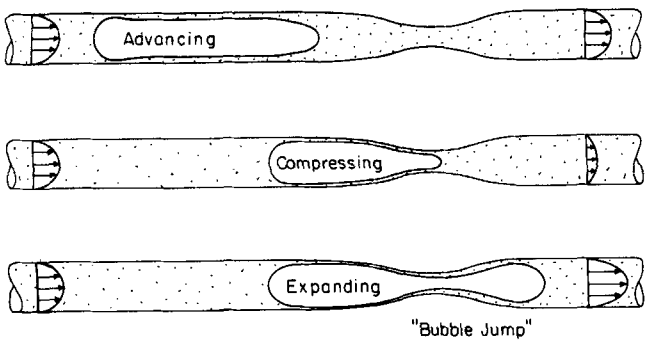

Figure 2. Movement of compressible bubbles in constricted capillaries.

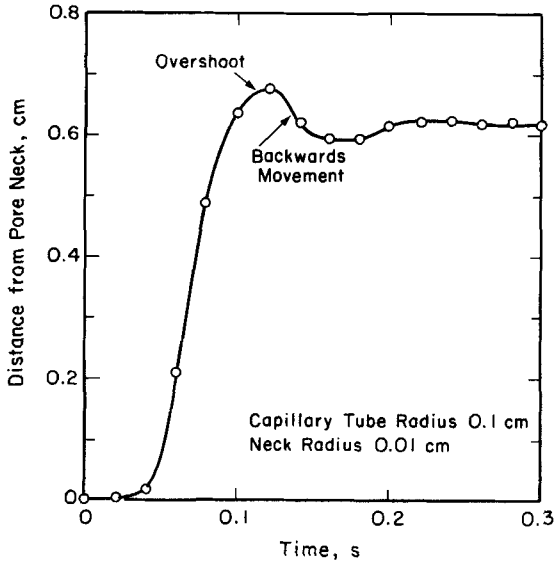

Figure 3. Experimental observation of a gas bubble jumping into water.
Position of bubble front from pore neck is shown as a function of time; bubble overshoots its equilibrium position and then moves backward.

thickness of the liquid film deposited by the bubble, steps 1, 2, 3 of Figure 1. The film thickness, in turn, determines the flow rate of liquid into the growing collar. The wetting fluid viscosity, μ, and the surface tension, σ, are equally important. However, these are physical properties that can be controlled, or at least measured. In contrast, the velocity of the bubble jump is unknown. The objective of this work is to quantify the velocity of the Haines jump and to determine how gas compressibility affects snap-off of gas bubbles.

Previous Work

The impulsive motion of the oil/water interface is important in the mobilization and subsequent flow of nonwetting oils in porous media. Ng et al. (1978) indicate that the Ohnesorge number, $Oh = \mu/(\rho\sigma R_T)^{1/2}$, dictates whether the unsteady motion is a slow viscous ooze, or a fast impulsive motion that is dominated by inertia. The Ohnesorge number is a ratio of viscous forces to inertial and surface tension forces. For large Oh, viscous forces damp the motion; for small Oh values, inertial forces dominate, and the motion is impulsive.

Mohanty (1981) presents a scaling analysis to determine the characteristic velocity of an oil drop that jumps from a pore neck into a pore body. As expected, the Ohnesorge number characterizes the dynamics of the bubble jump.

Levine et al. (1980) developed a quantitative analysis to follow the unsteady capillary rise in a periodically constricted capillary. Inertia causes the meniscus to overshoot its steady state position, to perhaps another metastable configuration, and then oscillate about its final position. Inertial effects cause the oscillations, which are subsequently damped by viscous dissipation. Legait et al. (1983) presented a theory for the impulsive motion of an oil drop displaced by water in a constricted capillary. Inertia also caused oscillations about steady state positions. In these studies, viscous dissipation was obtained by assuming fully developed flow. However, for rapid movements where inertia is

important, such as accelerating Poiseuille flow (Bird et al., 1960), velocity profiles are not fully developed. The motivation for this comment will resurface in the section on comparison with experimental data.

In this investigation, a detailed hydrodynamic analysis is presented to determine, in particular, the role of gas compressibility on the capillary number of the Haines jumps. We consider only the important part of the bubble movement: the bubble jump downstream from the constriction. In the next section, the unsteady, impulsive motion is analyzed with a macroscopic momentum balance. Following that, numerical solution of the momentum balance is reported. Finally, theory is compared with existing experimental data for the position of the bubble front as a function of time, and the role of gas compressibility and the Ohnesorge number in bubble snap-off is rationalized.

Problem Statement

Since our interest is primarily in the bubble jumps, we determine only the motion of the bubble on the downstream side of the capillary. That is, we neglect the motion of the bubble upstream from the constriction, and assume that the bubble is at rest initially with its front at the neck of the constriction. Experimental observations confirm this approximation for bubbles driven at very low capillary numbers, $Ca_T \leq 5 \times 10^{-4}$, through constricted circular capillaries (Gauglitz, 1986; Gauglitz et al., 1988).

Consider a bubble front displaced a length h from the neck of a constricted capillary, as shown in Figure 4. Cylindrical coordinates (r, x) are employed with the axial origin $(x = 0)$ at the neck of the constriction. The radius of the unconstricted capillary is R_T, and the downstream length of the capillary measured from the neck of the constriction is L_T. The initial length of the bubble is h_o.

The shape of the constriction is given by an arbitrary dimensionless function $\lambda(x)$ where the slope of the pore wall $d\lambda R_T/dx \ll 1$. In this work, the following cosine function is employed,

$$\lambda(x) = 1 - a[1 + \cos(\pi x/R_T b)] \tag{1}$$

Parameters a and b determine the neck radius and the length of the constriction, respectively. We require the slope of the pore wall to be small so the classical lubrication approximation can apply (Denn, 1980; Batchelor, 1967).

Momentum balance

To follow the unsteady motion of the bubble, we employ a macroscopic momentum balance on the fluid downstream from the bubble front. The control volume is the region within the cylindrical capillary that lies between planes $P1$ and $P2$, indicated by the dashed lines in Figure 4. This is chosen for convenience since both the gas density and viscosity are small. In writing the unsteady macroscopic momentum balance in the axial direction, we assumed that:

1. Plane 1 of the control volume moves with the bubble front, so there is no flux of momentum into the control volume at this plane
2. The velocity of the fluid is coparallel with the axial direction, so the magnitude of the velocity is essentially equal to the axial component: $|v| \sim v_x$; *this is valid within the lubrication* approximation
3. The wetting liquid is incompressible and Newtonian with a constant density and viscosity

With these assumptions, the axial component of the macroscopic momentum equation (Denn, 1980) becomes

$$\begin{aligned} \rho \frac{d}{dt} \int_V \langle v_x \rangle \, dV = & -\rho A_2 \langle v_x^2 \rangle_2 && \text{momentum efflux} \\ & + P_1 A_1 && \text{entrance pressure force} \\ & - P_2 A_2 && \text{exit pressure force} \\ & + F_p && \text{pressure force along the capillary wall} \\ & - F_x && \text{viscous drag} \end{aligned} \tag{2}$$

where the symbol $\langle\ \rangle$ implies the average of the quantity over the cross section.

The first term on the lefthand side of Eq. 2 specifies the accumulation of momentum within the control volume. The remaining terms are described by the equation. A unique aspect of the momentum balance is that the axial component of the pressure exerted by the capillary wall on the liquid, F_p, must be included in the balance. This is an added, though not difficult, complication of applying a momentum balance to flow in a constricted capillary. F_p is discussed below.

We now express each term as function of the average velocity at plane 1, which is assumed to be equal to the velocity of the bubble front. Continuity relates the average velocity at any axial position to the velocity at plane 1 as follows:

$$\langle v_x(x) \rangle = \left[\frac{\lambda_1}{\lambda(x)}\right]^2 \langle v_x \rangle_1 = \left[\frac{\lambda_1}{\lambda(x)}\right]^2 \frac{dh}{dt} \tag{3}$$

where λ_1 is the dimensionless capillary radius at the bubble front: plane 1.

The total force exerted by the fluid on the capillary wall is given by the following integral,

$$F_x = \int_1^2 \tau_w 2\pi\lambda R_T \, dx \tag{4}$$

Within the lubrication approximation, the viscous drag at the wall, τ_w, is determined by assuming Poiseuille flow locally to yield:

$$\tau_w = 4\mu \frac{\langle v_x \rangle}{\lambda R_T} \tag{5}$$

where $\langle v_x \rangle$ is the average axial velocity that varies along the capillary. Combining Eqs. 3 through 5 gives the total viscous

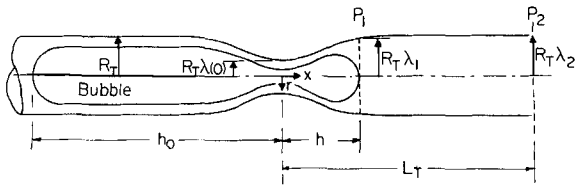

Figure 4. Gas bubble inside a constricted capillary just after expansion into downstream region.
Initial bubble length is h_o; rear of bubble remains stationary.

drag in terms of $\langle v_x \rangle_1$:

$$F_x = 8\pi\mu\langle v_x\rangle_1\lambda_1^2 \int_1^2 \frac{dx}{\lambda^2(x)} \tag{6}$$

A useful dimensionles pore-shape integral S_1 is defined by

$$S_1 \equiv \int_1^2 \frac{d\tilde{x}}{\lambda^2(\tilde{x})} \tag{7}$$

where $\tilde{x} = x/R_T$.

For the momentum efflux term, the liquid exits the capillary at plane 2 into a liquid bath. Here, we assume the velocity is uniform plug flow, so the average of v_x^2 at plane 2 is the square of the average. Considering Eq. 3, the momentum efflux term becomes

$$\rho A_2\langle v_x^2\rangle_2 = \rho\pi R_T^2 \frac{\lambda_1^4}{\lambda_2^2}\langle v_x\rangle_1^2 \tag{8}$$

Assuming a parabolic flow profile at the capillary exit makes the average of v_x^2 a factor 4/3 larger than the square of the average velocity (Denn, 1980). However, the difference between our assumed value of 1 and 4/3 is immaterial in later calculations because the downstream section of the capillary is quite long and viscous drag swamps the momentum efflux. The exit pressure, P_2, in Eq. 2 is influenced by flow rearrangement at the capillary exit. However, an exit correction only contributes additional drag equivalent to a length of capillary less than one diameter long. Because the downstream section of the capillary is long, this exit correction is immaterial and is neglected.

The accumulation of momentum requires the integration of the average velocity over the control volume. Expressing the average velocity with Eq. 3 leads to

$$\int_V \langle v_x\rangle\, dV = \int_1^2 \langle v_x\rangle \pi R_T^2\lambda^2(x)\, dx = \pi R_T^2\lambda_1^2\langle v_x\rangle_1(L_T - h) \tag{9}$$

Mass continuity dictates that the product of cross-sectional area and average velocity must be a constant. Accordingly, Eq. 9 shows that the momentum per unit axial length is constant along the capillary, although it does vary in time. The momentum accumulation becomes

$$\rho\frac{d}{dt}\left[\int_V \langle v_x\rangle\, dV\right] = \rho\pi R_T^2\lambda_1^2\frac{d}{dt}\left[\langle v_x\rangle_1(L_T - h)\right] \tag{10}$$

where $\lambda_1(x)$ is not a function of time.

The pressure forces acting on planes 1 and 2 of the control volume are simply P_1 and P_2 as given in Eq. 2. Determining the axial component of pressure exerted by the capillary wall on the control volume is more involved. First, the pressure along the capillary (it is assumed constant across the cross section by the lubrication approximation) is determined from local Poiseuille flow as follows (Denn, 1980):

$$-\frac{dP}{dx} = \frac{8\mu}{(R_T\lambda)^2}\langle v_x\rangle \tag{11}$$

Combining with Eq. 3 and integrating from plane 1 to x gives

$$P(x) = P_1 - \frac{8\mu\langle v_x\rangle_1\lambda_1^2}{R_T^2}\int_1^x \frac{dx}{\lambda^4(x)} \tag{12}$$

Equations 11 and 12 assume fully developed flow. However, for rapid changes in velocity, fluid inertia alters the velocity profile, and thus the viscous drag.

Next, the component of this pressure force in the axial direction is needed. In the straight section of the capillary, the component in the axial direction is zero. For the constricted sections of the capillaries, geometry shows that the component of force in the axial direction is obtained by combining $P(x)$ with the following axial component of a differential area segment: $(2\pi R_T^2)\lambda(d\lambda/dx)dx$. Thus, the pressure force is written as

$$F_p = 2\pi R_T^2\int_1^2 P(x)\lambda\frac{d\lambda}{dx}\,dx = \pi R_T^2(\lambda_2^2 - \lambda_1^2)P_1 - 16\pi\mu\langle v_x\rangle_1\lambda_1^2\int_1^2\left[\int_1^x \frac{1}{\lambda^4}\,d\xi\right]\lambda\frac{d\lambda}{dx}\,dx \tag{13}$$

where the first term results from noting that $2\int_1^2 \lambda(d\lambda/dx)\,dx = \lambda_2^2 - \lambda_1^2$. We define a second dimensionless pore-shape integral S_2 by

$$S_2 \equiv \int_1^2\left[\int_1^{\tilde{x}} \frac{1}{\lambda^4}\,d\tilde{\xi}\right]\lambda\frac{d\lambda}{d\tilde{x}}\,d\tilde{x} \tag{14}$$

where again $\tilde{x} = x/R_T$ and $\tilde{\xi} = \xi/R_T$, and ξ is a dummy variable in the integration.

Gas compressibility

We consider the bubble to be initially at rest with the bubble front at the neck of the constriction, but the gas is compressed due to the curvature of the bubble front. The liquid pressure P_1 is related to the pressure in the gas by the Young-Laplace equation as follows (Adamson, 1976):

$$P_1 = P_g - \frac{2\sigma}{\lambda_1 R_T}\left[1 + 1.79\left(\frac{3\mu\langle v_x\rangle_1}{\sigma}\right)^{2/3}\right] \tag{15}$$

The velocity correction to the interfacial curvature results from a thin film of liquid deposited by the bubble which increases that curvature slightly (Park and Homsy, 1984; Bretherton, 1961). This correction is small. We assume that the density and viscosity of the gas are small so the gas pressure, P_g, is uniform throughout the bubble.

For expansion (or contraction) where no mass enters or leaves the gas bubble, the ideal gas law relates the gas pressure to the bubble volume as follows:

$$P_g V_B^\gamma = k \tag{16}$$

where $\gamma = 1$ represents isothermal expansion, and $\gamma = 1.4$ reflects adiabatic expansion (Smith and Van Ness, 1959). The constant k defines the mass (i.e., size) of the gas bubble. Combi-

nation of Eqs. 15 and 16 gives

$$P_1 = \frac{k}{\left[\pi R_T^2 \int_{-h_o}^{h} \lambda^2 dx\right]^\gamma} - \frac{2\sigma}{\lambda_1 R_T}\left[1 + 1.79\left(\frac{3\mu\langle v_x\rangle_1}{\sigma}\right)^{2/3}\right] \quad (17)$$

where the integral specifies the bubble volume, neglecting the hemispherical endcaps. The axial position $-h_o$ represents the location of the bubble back; we assume that h_o is a constant, so the bubble back does not move. Our visual observations indicate that during the Haines jump, the position of the bubble back remains fixed.

The constant k is determined from the initial bubble pressure and volume. Initially, the bubble is at rest with its front at the neck of the constriction. The initial gas pressure, P_g^i, is determined from the Young-Laplace equation (Adamson, 1976),

$$P_g^i = P_2 + \frac{2\sigma}{R_T\lambda(0)} \quad (18)$$

The initial volume is given by

$$V^i = \pi R_T^2 \int_{-h_o}^{0} \lambda^2 \, dx \quad (19)$$

Thus, k is given by

$$k = P_g^i (V^i)^\gamma \quad (20)$$

Dimensionless momentum balance

Time, t, is scaled with an inertial time scale $(\rho R_T^3/\sigma)^{1/2}$ to give the dimensionless time,

$$\tilde{t} = \frac{t}{(\rho R_T^3/\sigma)^{1/2}} \quad (21)$$

while the dimensionless lengths are

$\tilde{h} = h/R_T$, position of bubble front

$\tilde{h}_o = h_o/R_T$, initial bubble length

$\tilde{x} = x/R_T$, axial position originating at the pore neck

$\lambda(\tilde{x}) \equiv$ radial position of capillary wall

$\tilde{L}_T = L_T/R_T$, downstream length of capillary

These reduced quantities combined with Eqs. 2 through 21 give the following dimensionless equation describing the dynamic position of the bubble front $\tilde{h}$:

$$\frac{d}{d\tilde{t}}\left[(\tilde{L}_T - \tilde{h})\frac{d\tilde{h}}{d\tilde{t}}\right] = -\left(\frac{\lambda_1}{\lambda_2}\right)^2\left(\frac{d\tilde{h}}{d\tilde{t}}\right)^2 - Oh(8S_1 + 16S_2)\frac{d\tilde{h}}{d\tilde{t}} - P(\lambda_2/\lambda_1)^2 + \left(\frac{\lambda_2}{\lambda_1}\right)^2 \left\{\left(\tilde{P} + \frac{2}{\lambda(0)}\right)\left[\frac{\int_{-\tilde{h}_o}^{0}\lambda^2 d\tilde{x}}{\int_{-\tilde{h}_o}^{\tilde{h}}\lambda^2 d\tilde{x}}\right]^\gamma - \frac{2}{\lambda_1}\left[1 + 1.79\left(3Oh\frac{d\tilde{h}}{d\tilde{t}}\right)^{2/3}\right]\right\} \quad (22)$$

The important dimensionless parameters are: the Ohnesorge number $Oh = \mu/(\rho\sigma R_T)^{1/2}$; the scaled exit pressure $\tilde{P} = P_2 R_T/\sigma$; the initial bubble length $\tilde{h}_o$; the length of the tube downstream from the constriction $\tilde{L}_T$, and the pore geometry, where the neck radius of the constriction, $\lambda(0)$, is most crucial. In addition, the pore shape integrals contain the function $\lambda(x)$. Two parameters, a, b, describe the pore shape.

The Ohnesorge number determines whether the bubble jump is fast and impulsive or slow and oozing. The scaled pressure $\tilde{P}$ determines if gas compressibility is important, and illustrates how laboratory experiments in capillaries where $R_T \sim 0.1$ cm are scaled to naturally occurring porous media where $R_T \sim 10^{-3}$ cm. The increase in gas pressure to move the bubble front into the constriction is represented by the factor $[\tilde{P} + 2/\lambda(0)]$, which originates from Eq. 18. In combination with the initial bubble volume $\int_{-\tilde{h}_o}^{0}\lambda^2 \, d\tilde{x}$, these parameters determine how far the bubble can expand into the downstream side of the constriction until it achieves an equilibrium configuration.

The capillary number of the Haines jump is crucial for bubble snap-off and is related to the velocity of the jump as follows:

$$Ca = \mu U/\sigma = Oh\frac{d\tilde{h}}{d\tilde{t}} \quad (23)$$

The dimensionless bubble velocity, $d\tilde{h}/d\tilde{t}$, depends implicitly on the Ohnesorge number: the velocity decreases with increasing Oh. Accordingly, the dependence of the capillary number on the Ohnesorge number given in Eq. 23 is not linear.

Model parameters can be directly related to quantities characteristic of gas bubbles in porous media, and the dimensionless groups dictate the relevant scaling. The mean reservoir pressure is equivalent to P_2, the pore body radius is R_T, and the pore shape is $\lambda(x)$. The initial bubble length, h_o, is related to the average bubble size of a foam. Physical properties depend on the reservoir fluids, temperature, and pressure. The length of the downstream capillary, $\tilde{L}_T$, is more difficult to relate directly to porous media. However, it does reflect the amount of downstream wetting liquid attributable to a pore neck.

Numerical procedure

Equation 22 is a nonlinear, second-order ordinary differential equation. It is an initial-value problem, so two initial conditions are prescribed. These are that the bubble front is stationary and is located at the neck of the constriction. Since this is a stable configuration, we start the bubble front slightly downstream from the constriction. The initial conditions are given by

$$\tilde{h}(\tilde{t}) = +\epsilon \quad \text{at } \tilde{t} = 0 \quad (24)$$

$$\frac{d\tilde{h}(\tilde{t})}{d\tilde{t}} = 0 \quad \text{at } \tilde{t} = 0 \quad (25)$$

where ϵ is a small constant typically chosen to be 0.5. Interestingly, the position of the bubble front is stable to infinitesimal movements away from the pore neck. This results because the capillary is essentially straight near the pore neck, and the bubble pressure decreases more than the curvature decreases for small perturbations about $\tilde{x} = 0$. The axial position of 0.5 is a sufficient displacement to cause the bubble to expand into the downstream region of the capillary rather than recede into the constriction. The phenomenon is specific for compressible bub-

bles where the back of the bubble is fixed, and for the pore constriction shape [i.e., $\lambda(\tilde{x})$] used in these calculations.

A fourth-order Runge-Kutta method is employed to integrate Eq. 22 in time (Lapidus, 1962). The trapezoidal rule evaluates the pore-shape integrals $S_{1,2}$ (Lapidus, 1962). Further details on the numerical methods are given by Gauglitz (1986).

Results and Discussion

The movement of the bubble front as the bubble expands downstream from a constriction is shown in Figure 5. Here, the dimensionless pressure of $\tilde{P} = 2{,}875$ corresponds to a capillary with $R_T = 0.2$ cm and atmospheric pressure at the capillary exit. The bubble begins wth its front slightly displaced from the constriction. In this calculation, $\epsilon = 0.1$ rather than the typically chosen value of $\epsilon = 0.5$. The bubble moves forward into the downstream section of the capillary as time increases until equilibrium is established.

The downstream equilibrium position depends on the amount the bubble is compressed (the origin of this lies in Eq. 18), on the value of γ, which we set to unity, and on the size of the initial upstream bubble. The radius at the neck of the constriction, $\lambda(0)$, and the dimensionless pressure, $\tilde{P}$, determine the amount of compression. The amount of gas in the bubble is fixed, indicated by the constant k in Eq. 20, and the downstream equilibrium position corresponds to a larger bubble volume but lower pressure, which achieves the same value of k. Thus, the bubble moves downstream from the constriction to where the gas pressure and the bubble volume combine to give the same value of k.

Bubble dynamics depend on the Ohnesorge number. For a large Ohnesorge number, $Oh = 0.1$ in Figure 5, the bubble moves smoothly toward the downstream equilibrium position. This corresponds to a viscous ooze; inertial effects are negligible.

When the Ohnesorge number is small, Figure 5 demonstrates how inertia influences the movement of the bubble toward the final position. For $Oh = 0.02$, the bubble front accelerates out of the constriction very quickly. Due to the inertia of the downstream liquid, the bubble front is carried beyond its final equilibrium position. Here, the pressure in the bubble is below its equilibrium value so the bubble contracts, causing the front to move backwards. This is indicated by the decrease in the position of the bubble front when $20 < \tilde{t} < 45$ in Figure 5. The slope of the curve is also negative, corresponding to a negative velocity and backward motion. The bubble front oscillates about the final position due to inertia, and viscous dissipation decreases the amplitude of the oscillations.

For the intermediate Oh value of 0.05 shown in Figure 5, the bubble front slightly overshoots the final position, again due to inertia. The bubble front then recedes toward the final position without oscillations. All these results are typical of Haines jumps driven by a compressible bubble. However, the magnitude of the oscillations, and the time required for bubbles to approach the final position, depend on the model parameters.

Figure 6 shows the bubble movement in a smaller radius capillary, indicated by a $\tilde{P}$ value of 750. In addition, both the neck radius of the constriction and the downstream capillary length are larger. Dimensionless time still ranges from 0 to 80 for comparison with Figure 5. The curve for $Oh = 0.02$ indicates a viscous ooze to the final position of $\tilde{h} \sim 10$, and the Oh value of 0.005 demonstrates oscillations about the final position. These

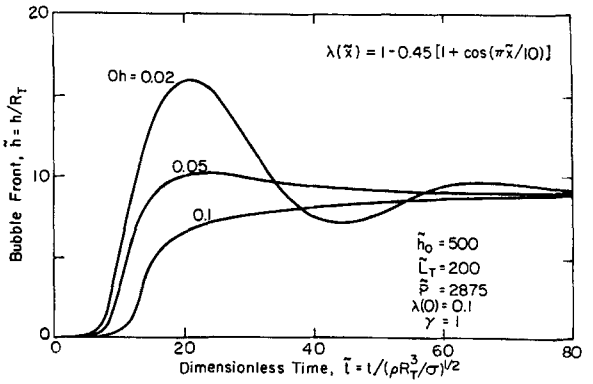

Figure 5. Bubble front position during expansion into downstream section of capillary.

At high Oh values motion is a slow viscous ooze; at low Oh values, motion is an inertially dominated Haines jump; oscillations are a result of inertia.

results are similar to those reported in Figure 5. However, for the Oh value of 0.02, Figure 5 indicates considerable oscillations, but Figure 6 shows a viscous ooze. Therefore, for comparison with experimental data, it is important to characterize the capillary geometry as well as the liquid properties.

A series of calculations for various parameter values shows the following trends

1. Increasing the upstream bubble size, decreasing the neck radius of the capillary, or decreasing $\tilde{P} = P_2/(\sigma/R_T)$:

- Increases the axial position of the bubble front in its final equilibrium configuration
- Increases the velocity of the jump

2. Increasing the length of the downstream capillary:

- Decreases the velocity of the jump
- Damps the oscillations at smaller Oh values more quickly.

When $\gamma = 1.4$, compared to $\gamma = 1$, the final equilibrium position of the bubble front is less, see Eq. 16. Physically, the temperature in the gas decreases during an adiabatic expression, and accordingly, a smaller bubble volume gives the same value of k in Eq. 16.

Haines jumps due to gas expansion are important because of their dramatic effect on bubble snap-off in constricted capillar-

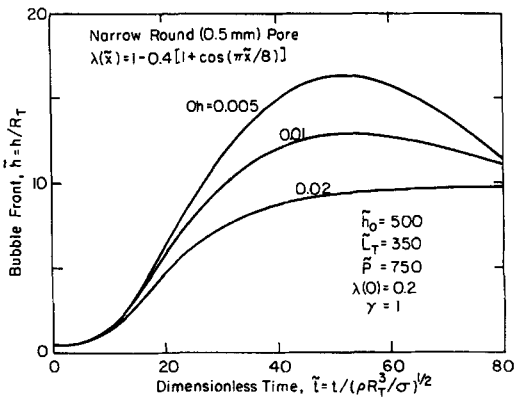

Figure 6. Bubble front position during expansion into downstream section of capillary.

Effects of a longer downstream capillary, a larger radius at the constriction, and a smaller unconstricted capillary radius are illustrated with relation to Figure 5.

ies (Gauglitz, 1986; Gauglitz and Radke, 1987; Gauglitz et al., 1988). These previous studies demonstrate that the rapid Haines jumps, step 3 of Figure 1, deposit a relatively thick liquid film. This thicker film flows into the capillary neck, causing snap-off faster than predicted theoretically if the Haines jump is neglected.

The most important parameter in bubble snap-off is the capillary number, defined by Eq. 23. It determines the thickness of the wetting liquid film deposited by the bubble (Bretherton, 1961; Taylor, 1961; Fairbrother and Stubbs, 1935). A thicker film allows liquid to flow into a constriction more quickly causing faster bubble snap-off. Therefore, a number of calculations are reported in Figure 7 showing the effect of the Ohnesorge number, and the other physical parameters, on a characteristic capillary number. We report the maximum capillary number, Ca_m, determined with Eq. 23 and the maximum slope of the bubble position as a function of time. Ca_m is defined as follows:

$$Ca_m \equiv Oh \left(\frac{d\tilde{h}}{d\tilde{t}}\right)_m \tag{26}$$

Figure 7 shows the maximum capillary number for a range of Ohnesorge numbers. All the curves asymptote to a constant capillary number when $Oh > 0.2$. This limit corresponds to a viscous ooze, and accordingly, inertia has negligible influence on the velocity of the Haines jump. In this regime, the capillary number is independent of the Ohnesorge number. For small Oh values, $Oh < 10^{-2}$, inertia dominates the velocity of the jump. As discussed in a previous analysis (Gauglitz, 1986; Gauglitz et al., 1988), the characteristic velocity of an inertial jump is $U_{char} = O[(\sigma/R_T\rho)^{1/2}]$. Combined with Eq. 23, the characteristic capillary number of an inertial jump is of the order of the Ohnesorge number:

$$Ca_{char} = \mu U_{char}/\sigma = O(Oh) \tag{27}$$

This illustrates why the slope of the curves in Figure 7 are unity when $Oh < 10^{-2}$ and inertia dominates the Haines jumps.

As seen in Figure 7, the dimensionless length of the initial bubble ranging from 100 to 500 has only a small influence on the maximum capillary number of the Haines jump. This is true for initial bubble sizes sufficiently large to give bubble jumps at least a few tube diameters downstream from the constriction.

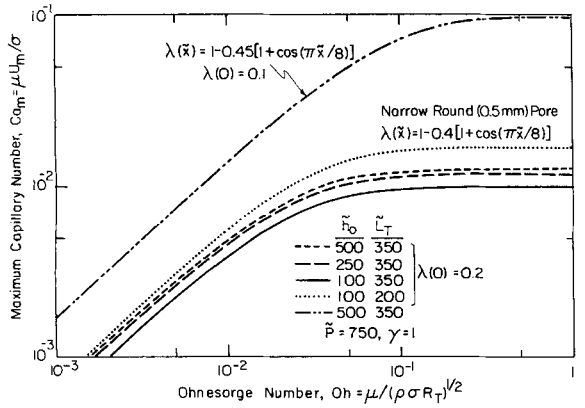

Figure 7. Effect of Ohnesorge number on maximum capillary number.

Increasing the initial bubble length further from 500 to 1,500 increases the maximum capillary number by less than 1%. However, the initial bubble length does determine the final equilibrium position of the bubble front. Decreasing the length of the downstream capillary from 350 to 200 increases the capillary number by an amount that is essentially proportional to the fractional decrease in tube length. This results from the decrease in the viscous dissipation because the capillary is shorter. Changing the neck radius of the capillary, however, has a dramatic affect on the capillary number. Decreasing the neck radius from $\lambda(0) = 0.2$ to $\lambda(0) = 0.1$ increases the capillary number by a factor of 5 to 10. This results because the smaller constriction demands an increased gas pressure, and hence, an increased pressure driving force for flow.

Comparison with Experimental Data

Recent experimental investigations have quantified the movement and breakup of gas bubbles in constricted cylindrical capillaries (Gauglitz, 1986; Gauglitz et al., 1988). A glass-windowed viewing cell, containing a solution that matches the refractive index of the glass capillaries, both holds the capillaries and allows undistorted visual observation of bubbles as they move through the constriction. Sixteen mm motion pictures record the observations. By viewing the film frame by frame, the dynamics of the bubble motion and the time required for the growing collar at the pore neck to snap off are determined. The reader is referred to Gauglitz (1986) and Gauglitz et al. (1988) for experimental details on the apparatus and filming procedure. We discuss here only data for surfactant-free solutions where surface tension gradient effects are negligible.

A stringent test for the macroscopic momentum balance is predicting the position of the bubble front as a function of time. Figure 8 shows a comparison of theory and experiment for an air bubble in a constricted capillary designated the *narrow round* (0.5 mm) *pore*. The pore shape is accurately represented by the cosine function written in the figure. The fluid is a mixture of glycerol in water with a viscosity of 8.5 mPa · s. The bubble moves through the upstream section of the capillary at $Ca_T = \mu U_T/\sigma = 5 \times 10^{-5}$ where U_T is the bubble velocity in the straight section of the capillary. The first datum at $\tilde{t} = 0$ is when the bubble front is at the neck of the constriction. The parameters in

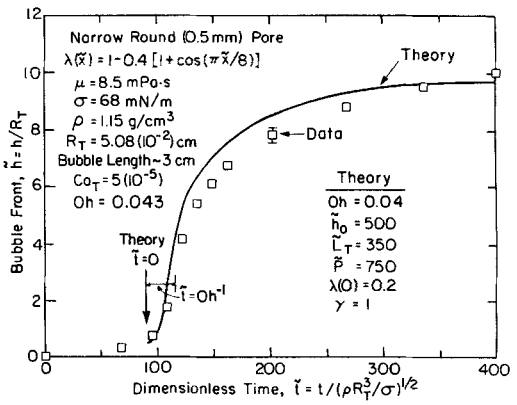

Figure 8. Comparison of macroscopic momentum balance, Eq. 22, with experimental data for position of bubble front as a function of time.
Solution is 8.5 mPa · s glycerol/water mixture.

the theory correspond exactly to the experimental parameters, with the exception of the initial bubble length, $\tilde{h}_o$. We have chosen the bubble length as 500 to match with the experimentally observed final equilibrium position. The equilibrium position is larger than expected due to extraneous compression within the experimental apparatus in addition to the air bubble. Although care was taken to remove all other air bubbles, it is apparent from the experimental equilibrium position that extra compression occurs in the apparatus. Additionally, bubble jumps were observed for a range of initial bubble volumes (0.02 to 2.0 cm^3) and, as expected, the larger bubbles gave rise to longer jumps. For larger bubbles the extraneous compression should be less important, but quantitative comparison of theory with data for larger bubbles is difficult because snap-off interrupts the jump.

The theoretical calculation begins with the bubble front at an initial position of $\tilde{h} = 0.5$. To compare with the experimental data that locate the bubble front at $\tilde{h} = 0$ at $\tilde{t} = 0$, we redefine the initial time in the calculation to start at $\tilde{t} = 85$. This time corresponds to the experimentally observed position for the bubble front being $\tilde{h} = 0.5$. As Figure 7 shows, for sufficiently large bubbles the initial bubble size has only a slight influence on the bubble velocity; its primary effect is to shift the axial position of the equilibrium configuration. Therefore, choosing a bubble size to correspond with the data does not affect the slope of the curve or its position as a function of time. Considering the approximations in the analysis, Figure 8 shows that agreement between theory and experiment is good, once the correct bubble size is set.

The macroscopic momentum balance is compared with experimental data for an air bubble displacing a 1.0 mPa · s viscosity liquid in Figure 9. Data show the bubble jumping to a final axial position of $\tilde{h} \sim 16$. In the theory, an initial bubble length of $\tilde{h}_o = 1{,}500$ is chosen for comparison, which predicts an equilibrium position farther downstream than indicated by the data. However, the bubble size does not affect strongly the maximum velocity of the bubble jump, so any reasonable bubble length can be chosen for comparison with experiments.

The theoretical curve for $Oh = 5 \times 10^{-3}$ corresponds to the physical properties of water. Clearly, the theoretical curve for $Oh = 2 \times 10^{-2}$ gives a much better fit to the data. Although theory compares well for the 8.5 mPa · s viscosity solution shown in Figure 8, the theory in Figure 9 for $Oh = 5 \times 10^{-3}$ predicts a large oscillation in the bubble position that is not observed experimentally. Thus, agreement between the macroscopic momentum balance and data is poor for the 1.0 mPa · s viscosity fluid. It is apparent from Figure 9 that increasing the viscous dissipation by a factor of four, which is equivalent to increasing the Ohnesorge number from 5×10^{-3} to 2×10^{-2}, gives reasonable agreement with experimental data.

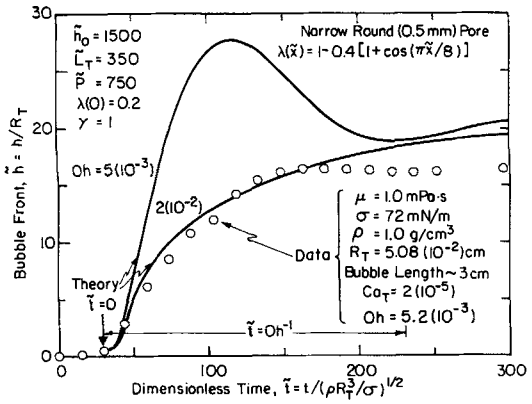

Figure 9. Comparison of macroscopic momentum balance, Eq. 22, with experimental data for position of bubble front as a function of time.

Liquid is 1.0 mPa · s deionized/water.

We assert that the discrepancy between theory and experiment in Figure 9 results from the parabolic velocity profile used to estimate the viscous dissipation and pressure drop, Eqs. 5 and 11. The effect of each parameter in the equation was investigated, as described earlier, and only increasing the viscous dissipation (i.e., by increasing Oh or $\tilde{L}_T$) leads to agreement between theory and data at low Oh values. Since Oh and $\tilde{L}_T$ are known experimentally, the only plausible cause for the difference between theory for the oscillation magnitude and data in Figure 9 is the assumed parabolic velocity profile. This profile is not appropriate for the 1.0 mPa · s viscosity fluid because a fully parabolic velocity profile has not developed during the short time scale of the Haines jump. However, fully developed Poiseuille flow is appropriate for the 8.5 mPa · s viscosity solution.

Consider the acceleration of a fluid in a cylindrical capillary from rest under an applied pressure gradient as discussed by Bird et al. (1960). As the fluid accelerates, the velocity profile is initially flat, but approaches a parabolic profile as time increases. The velocity relaxes to a parabolic profile over a time scale given by

$$\frac{\mu t}{\rho R_T^2} = O(1) \tag{28}$$

In the units of dimensionless time given by Eq. 21, this time scale corresponds to $\tilde{t} = Oh^{-1}$. The duration of the Oh^{-1} time period is shown in Figure 9 to demonstrate that the bubble jump occurs over a shorter time scale and that the velocity profile is not fully developed. Early time velocity profiles are flat, as depicted in Figure 10. For the same average velocity, the flatter profile gives a higher shear stress on the wall of the capillary. Accordingly, the viscous dissipation is larger. Clearly, during the initial stages of the jump, the shear stress at the wall is much larger than that given in Eqs. 5 and 11. Since the data agree well with theory for an Ohnesorge number of 2×10^{-2}, increasing the viscous dissipation by a factor of four appears correct for this value of the Ohnesorge number. For comparison, the time scale of $\tilde{t} = Oh^{-1}$ is also shown in Figure 8 for the 8.5 mPa · s viscosity solution. Here, the Haines jump occurs over a time scale much longer than $\tilde{t} = Oh^{-1}$, and fully developed parabolic flow is a good assumption. Accordingly, the macroscopic momentum bal-

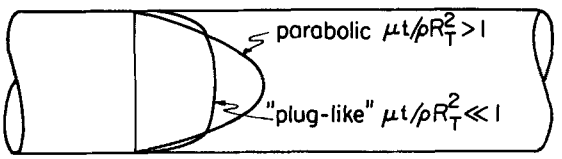

Figure 10. Fully developed parabolic velocity profile and early time flat profile.

Both profiles have the same average velocity; shear stress at the wall is greater for the flat profile.

ance, Eq. 23, accurately represents the Haines jumps in Figure 8.

When inertia causes bubble oscillation at low values of *Oh*, it also alters the fluid velocity profile from the steady-flow parabolic profile. So although the oscillations are due to inertia, our theory will be inaccurate whenever oscillations occur. The analyses of Levine et al. (1980) and Legait et al. (1983) for unsteady flow in constricted capillaries also assume fully developed flow, and thus have this same limitation. For an accurate theory of inertial oscillations, one must solve the time-dependent Navier-Stokes equations rather than assume a steady-flow result for the viscous drag.

The data in Figure 3 ($Oh = 3.7 \times 10^{-3}$) for a more tightly constricted capillary [$\lambda(0) = 0.1$] clearly demonstrate oscillations. Again, the magnitude of the oscillations is considerably less than theory predicts.

Snap-off of gas bubbles

As mentioned in the introduction, Haines jumps affect the time to snap-off of gas bubbles as they move through constricted capillaries. In a series of previous analyses (Gauglitz, 1986; Gauglitz et al., 1988; Gauglitz and Radke, 1987), it is shown that the capillary number is crucial for quantifying the time required for a wetting collar to grow at a pore neck and snap off a bubble. Dimensionless time to breakup, $\tau_b = t_b/(3\mu R_T/\sigma)$, varies with the capillary number to the -2 power. In the appendix we repeat the qualitative physical arguments given by Gauglitz et al. (1988) that justify this capillary number dependence. For a Haines jump, we adopt the maximum capillary number given in Figure 7 since it is characteristic of the jump. This gives the following equation for the time to breakup:

$$\tau_b = \beta Ca_m^{-2} \tag{29}$$

where β is a constant that must be determined theoretically or experimentally.

The experimental studies of Gauglitz (1986) and Gauglitz et al. (1988) report the time to breakup for a series of glycerol in water mixtures with different initial bubble lengths. Sixteen mm motion pictures are used to record bubble movement through constricted capillaries. By viewing the film frame by frame, the position of the bubble front as a function of time and the time to breakup can be measured. To determine the bubble velocity, and therefore the bubble capillary number, Gauglitz (1986) fits the position of the bubble front vs. time data with cubic spline functions (Hornbeck, 1975; Carnahan et al., 1969). The derivative of the spline functions gives the bubble velocity. Experimental data for the capillary number of the Haines jumps, such as those in Figure 8, are reported by Gauglitz et al. (1988). In Figure 8, the measured capillary number has a maximum of 8×10^{-3}. The measured dimensionless time to breakup for this case is $\tau_b = 6 \times 10^3$. With Eq. 29, we calculate that $\beta = 0.38$. This gives an experimental determination of β. From the measured bubble velocities and an extended film evolution equation, Gauglitz (1986) has determined semitheoretically a β value of 9.6×10^{-2}. This theoretical value is four times smaller than the corresponding experimental value.

To allow accurate comparison with experimental breakup time data, we use $\beta = 0.38$: the experimental determination. The maximum capillary number presented in Figure 7 can now be used to predict the time to breakup when Haines jumps are important. Figure 11 plots data (see Figure 16 of Gauglitz et al., 1988, or Gauglitz, 1986) and theory for the time to breakup vs. the Ohnesorge number for a series of different initial bubble lengths. The theory curves are obtained with Eq. 29 ($\beta = 0.38$) and the calculated results in Figure 7. At low *Oh* values, theory predicts that the time to breakup is proportional to the Ohnesorge number to the -2 power: the inertial limit. At high *Oh* values, the time to breakup approaches a constant: the viscous oozing limit. The experimental data for ~8 cm long bubbles show the excellent agreement with theory, clearly confirming our predictions. In agreement with all the experimental data, theory demonstrates the slight dependence of the initial bubble length on the time to breakup. Figure 7 shows that the maximum capillary number depends weakly on the initial bubble length; this is the origin of the length dependence in Figure 11.

Assuming that the time to breakup is proportional to the inverse square of a capillary number, simplifies the complicated hydrodynamics of gas-bubble snap-off. The evolution equation of Gauglitz and Radke (1987) can follow the details. However, Eq. 29 reflects the essence of bubble snap-off with Haines jumps. Although simple, it accurately represents experimental data for Ohnesorge numbers ranging from 5×10^{-3} to 0.3.

Conclusions

The dynamics of Haines jumps for compressible bubbles is quantified with a macroscopic momentum balance. Numerical solution of the momentum balance predicts the position of the bubble front as a function of time and the capillary number for the Haines jump. At low Ohnesorge numbers ($Oh < 10^{-2}$), the motion is impulsive and dominated by inertia. Oscillations of the bubble about a final equilibrium position are predicted as a consequence. For high Ohnesorge numbers ($Oh > 10^{-1}$), the motion is a viscous ooze. The maximum capillary number for the Haines jumps depends on the length of the capillary downstream from the constriction, on the shape of the pore constriction (primarily the neck radius), on a scaled downstream pressure $\tilde{P}$, and weakly on the size of the initial bubble. The size of

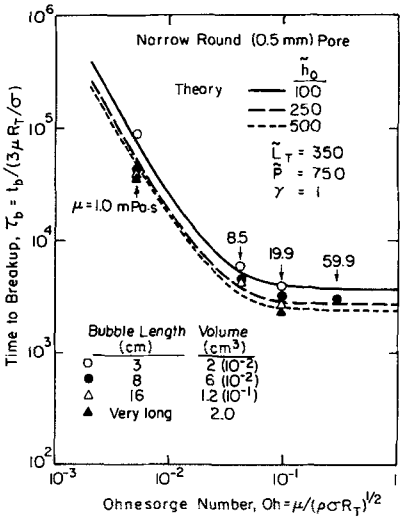

Figure 11. Effect of Ohnesorge number on time to breakup.

Experimental data from Gauglitz et al. (1988); solutions are glycerol/water mixtures.

the initial bubble specifies the equilibrium axial length the bubble can expand out of the constriction.

Comparison of experimental data with theory for the position of the bubble front as a function of time is excellent when the dimensionless time scale for the bubble jump is long compared to Oh^{-1}. Here, fully developed parabolic flow provides a good estimate for the viscous dissipation. When the Haines jumps occur quickly (i.e., the jump occurs within $\tilde{t} = Oh^{-1}$), theory predicts large oscillations that are not observed experimentally. When the jumps are this rapid, the velocity profile is flatter than the assumed parabolic profile, and the viscous dissipation is greater than predicted by local Poiseuille flow. Increasing the viscous dissipation by a factor of four gives good agreement with experimental data when $Oh = 5 \times 10^{-3}$.

The dimensionless time to breakup is proportional to the capillary number to the -2 power. Using the macroscopic momentum balance to predict the maximum capillary number of the Haines jumps gives excellent agreement with experimental breakup data for Oh values ranging from 5×10^{-3} to 0.3 over a range of initial bubble sizes.

Acknowledgment

This research was supported by the U.S. Department of Energy under Contract No. DE-AC03-76SF00098 to the Lawrence Berkeley Laboratory of the University of California. P.A. Gauglitz gratefully acknowledges financial support from the Shell Development Company.

Notation

$A_{1,2}$ = cross-sectional area at planes 1 and 2, m^2
a = parameter for determining neck radius of constriction
b = parameter for determining length of constriction
$Ca = \mu U/\sigma$, bubble capillary number
$Ca_{char} = \mu U_{char}/\sigma$, capillary number of inertial jump, Eq. 27
$Ca_m = Oh(d\tilde{h}/d\tilde{t})_m$, maximum capillary number of bubble jump, Eq. 26
$Ca_T = \mu U_T/\sigma$, tube capillary number
F_x = viscous drag force, N
F_p = pressure force along capillary wall, N
h = axial position of bubble front: $h = 0$ at $x = 0$, m
h_o = initial length of bubble, m
$\tilde{h} = h/R_T$, dimensionless axial position of bubble front
$\tilde{h}_o = h_o/R_T$, dimensionless initial length of bubble
L_T = length of capillary downstream from pore neck, m
$\tilde{L}_T = L_T/R_T$, dimensionless length of downstream capillary section
$Oh = \mu/(\rho\sigma R_T)^{1/2}$, Ohnesorge number
P_1 = liquid pressure at plane 1: bubble front, Pa
P_2 = liquid pressure at plane 2: capillary axis, Pa
$\tilde{P} = P_2/(\sigma/R_T)$, dimensionless liquid pressure at capillary exit
P_g = pressure inside the gas bubble, Pa
P_g^i = initial pressure inside the gas bubble, Pa
r = radial position, m
$\tilde{r} = r/R_T$, dimensionless radial position
R_T = radius of unconstricted capillary, m
S_1 = dimensionless pore-shape integral, Eq. 7
S_2 = dimensionless pore-shape integral, Eq. 14
t = time, s
$\tilde{t} = t/(\rho R_T^3)^{1/2}$, dimensionless time
t_b = time to breakup, s
$U_{char} = O[(\sigma/R_T\rho)^{1/2}]$, characteristic velocity of inertial jump
U_T = bubble velocity in upstream section of capillary, m/s
$|v|$ = magnitude of liquid velocity vector, m/s
v_x = axial component of velocity, m/s
$\langle v_x \rangle$ = average velocity in axial direction, m/s
V = control volume, m^3
x = axial position ($x = 0$ at pore neck), m
$\tilde{x} = x/R_T$, dimensionless axial position ($x = 0$ at pore neck)

Greek letters

β = proportionally constant, Eq. 29
γ = constant defining isothermal or adiabatic expansion, Eq. 16
δ = wetting film thickness deposited by bubble, m
ϵ = initial disturbance of bubble position
λ = dimensionless radial position of capillary wall, Eq. 1
μ = viscosity of wetting liquid, mPa · s
$\tilde{\xi} = \xi/R_T$, dimensionless dummy variable in integration
$\pi = 3.14159$
ρ = density of wetting liquid, kg/m^3
σ = surface tension, nN/m
$\tau_b = t_b/(3\mu R_T/\sigma)$, dimensionless time to breakup

Subscripts

m = maximum value
1 = quantity evaluated at plane 1: bubble front
2 = quantity evaluated at plane 2: capillary exit

Appendix: Effect of Capillary Number on Time to Breakup

The capillary number is crucial in bubble snap-off since it determines the thickness of the fluid film deposited by the bubbles as they translate through the capillary. Bretherton (1961) and Park and Homsy (1984) have shown that when $Ca \to 0$, the film thickness, δ/R_T, is of the order of the capillary number to the $\frac{2}{3}$ power:

$$\delta/R_T = O(Ca^{2/3}) \tag{A1}$$

Hammond (1983) has demonstrated that the characteristic response time for flow in thin liquid film is proportional to the inverse cubic power or the film thickness, so that

$$\tau_b \alpha (\delta/R_T)^{-3} \tag{A2}$$

Combination of Eqs. A1 and A2 specifies that the time to snap-off is proportional to the capillary number to the -2 power:

$$\tau_b \alpha Ca^{-2} \tag{A3}$$

In the final section discussing snap-off of gas bubbles, we chose the maximum capillary number of the Haines jump for evaluating Ca in Eq. A3.

Literature Cited

Adamson, A. M., *Physical Chemistry of Surfaces,* Wiley, New York (1976).
Batchelor, G. K., *An Introduction to Fluid Dynamics,* Cambridge Univ. Press, New York (1967).
Bird, R. B., W. E. Stewart, and E. N. Lightfoot, *Transport Phenomena,* Wiley, New York (1960).
Bretherton, F. P., "The Motion of Long Bubbles in Tubes," *J. Fluid Mech.,* **10,** 166, (1961).
Carnahan, B., H. A. Luther, and J. O. Wilkes, *Applied Numerical Methods,* Wiley, New York, 63 (1969).
Craig, F. F., Jr., *The Reservoir Engineering Aspects of Waterflooding,* SPE Monograph Ser., Am. Inst. Mech. Eng., New York (1971).
Denn, M. M., *Process Fluid Mechanics,* Prentice-Hall, Englewood Cliffs, NJ, 1980.
Fairbrother, F., and A. E. Stubbs, "Studies in Electroendosmosis. VI: The Bubble-Tube Method of Measurement," *J. Chem. Soc.,* **1,** 527 (1935).
Falls, A. H., G. J. Hirasaki, T. W. Patzek, P. A. Gauglitz, D. D. Miller, and J. Ratulowski, "Development of a Mechanistic Foam Simulator: The Population Balance and Generation by Snap-off," Paper No. *SPE 14961,* SPE Reservoir Engineering, **3**(3) 884 (1988).

Friedmann, F., and J. A. Jensen, "Some Parameters Influencing the Formation and Propagation of Foams in Porous Media," Paper No. *SPE 15087*, SPE California Regional Meet., Oakland (April, 1986).
Gauglitz, P. A., "Instability of Liquid Films in Constricted Capillaries: A Pore Level Description of Foam Generation in Porous Media," *Ph.D. Thesis*, Univ. Calif., Berkeley (1986).
Gauglitz, P. A., and C. J. Radke, "The Dynamics of Liquid Film Breakup in Constricted Capillaries," submitted, *J. Colloid Interf. Sci.* (1987).
Gauglitz, P. A., C. M. St. Laurent, and C. J. Radke, "Experimental Determination of Gas-Bubble Breakup in a Constricted Cylindrical Capillary," *Ind. Eng. Chem. Res.*, **27**(7), 1282 (1988).
Hammond, P. S., "Nonlinear Adjustment of a Thin Annular Film of Viscous Fluid Surrounding a Thread of Another within a Circular Cylindrical Pipe," *J. Fluid Mech.*, **137**, 363 (1983).
Hirasaki, G. J., and J. B. Lawson, "Mechanism of Foam Flow in Porous Media: Apparent Viscosity in Smooth Capillaries," *Soc. Petr. Eng. J.*, **25**, 176 (April, 1985).
Hornbeck, R. W., *Numerical Methods*, Quantum, New York (1975).
Lapidus, L., *Digital Computation for Chemical Engineers*, McGraw-Hill, New York (1962).
Legait, B., P. Sourieau, and M. Combarnous, "Inertia, Viscosity, and Capillary Forces during Two-Phase Flow in a Constricted Capillary," *J. Colloid Interf. Sci.*, **91**(2), 400 (1983).
Levine, S., J. Lowndes, and P. Reed, "Two-Phase Fluid Flow and Hysteresis in a Periodic Capillary Tube," *J. Colloid Interf. Sci.*, **77**(1), 253 (1980).
Mohanty, K. K., "Fluids in Porous Media: Two-phase Distribution and Flow," *Ph.D. Thesis*, Univ. Minnesota (1981).
Morrow, N. R., "Physics and Thermodyanmics of Capillary Action in Porous Media," *Ind. Eng. Chem.*, **62**, 32 (1970).
Ng, K. M., H. T. Davis, and L. E. Scriven, "Visualization of Blob Mechanics in Flow Through Porous Media," *Chem. Eng. Sci.*, **33**, 1009 (1978).
Park, C-W. and G. M. Homsy, "Two-Phase Displacement in Hele Shaw Cells: Theory," *J. Fluid Mech.*, **139**, 291 (1984).
Ransohoff, T. C., "Foam Generation in Constricted Noncircular Capillaries and in Bead Packs," M.S. Thesis, Univ. Calif., Berkeley (1986).
Smith, J. M., and H. C. Van Ness, *Introduction to Chemical Engineering Thermodynamics*, McGraw-Hill, New York (1959).

Manuscript received Sept. 10, 1986, and revision received Aug. 4, 1988.